Geophys. J. Int. (2006) **166,** 155–169 doi: 10.1111/j.1365-246X.2006.02805.x

Three-dimensional seismic reflection investigation of the upper crustal Winagami sill complex of northwestern Alberta, Canada

J. Kim Welford[1]* and Ron M. Clowes[2]

[1]*Department of Earth and Ocean Sciences, University of British Columbia, Vancouver, B.C., Canada*
[2]*Lithoprobe Secretariat, University of British Columbia, Vancouver, B.C., Canada*

Accepted 2005 September 20. Received 2005 August 29; in original form 2005 February 23

SUMMARY

Using a 3-D seismic reflection data set recorded by the Canadian petroleum exploration industry to 5.1 s two-way traveltime (∼15 km depth) in northwestern Alberta, the Winagami reflection sequence (WRS), an interpreted sill complex previously identified on Lithoprobe 2-D multichannel seismic reflection lines, is investigated to determine its 3-D geometry and reflective characteristics. Clear evidence of the top of the WRS emerges from the data set. Data sections outline a 3-D reflective sheet dipping to the southeast. From polarity comparisons with reflections from the sedimentary sequence, the reflective signature of the deep body is inferred to result from higher impedance material than the surrounding host rocks, thus reinforcing earlier interpretations that the deep reflections result from doleritic sills intruded into gneissic crystalline basement. Simple 1-D forward modelling reveals that the thickness of the sheet is on the order of 100 m throughout the survey region. From 3-D Kirchhoff forward modelling, a model of the reflective sheet is constrained between 11 and 16 km depth along the northwestern edge of the survey area. The absence of the Winagami reflections, and basement reflectivity in general, in the southeast of the survey region coincides with a positive aeromagnetic anomaly inferred to be caused by magmatic rocks. The presence of the magmatic rocks may have either influenced the geometry of the intrusion of the sills, overprinted their reflective signature or been co-magmatic, dependent upon the relative timing of emplacement of the two features. The Winagami sill complex appears to have been intruded horizontally into the crust during a period of tectonic compression. The emplacement of such deep Precambrian sills represents an under-appreciated mode of magmatic addition into the crystalline crust.

Key words: Alberta, continental evolution, deep seismic reflection, mafic sills, Precambrian, seismic modelling.

1 INTRODUCTION

From 2-D multichannel seismic reflection lines acquired in western Canada by Lithoprobe, sequences of coherent upper crustal reflectivity have been observed within the crystalline crust of northern Saskatchewan (Mandler & Clowes 1997), southern Alberta (Mandler & Clowes 1998) and northwestern Alberta (Ross & Eaton 1997). Due to similarities in the reflective geometries and characteristics of these sequences, imaged cross-cutting relationships in northwestern Alberta and nearby surface outcrops in northern Saskatchewan, these reflector sequences have been interpreted as mafic sill complexes. One of these sequences, the Winagami reflection sequence (WRS) of northwestern Alberta, equivalently referred to herein as the Winagami sill complex, is characterized by one to five bands of bright coherent reflections confined within a depth range of 9–24 km (3–8 s two-way traveltime (TWTT)) and appears to extend over an area of more than 120 000 km^2 (Ross & Eaton 1997). If the sill interpretation for the WRS is correct, this deep igneous feature is comparable in size to many of the world's large Phanerozoic igneous provinces (Coffin & Eldholm 1994). The considerable lateral extent of the inferred sill complex and its location within the upper crystalline crust underlying the Western Canada Sedimentary Basin, a locus of extensive oil and gas exploration, provided the impetus for seeking an industry-acquired 3-D seismic reflection data set to investigate the sequence. While studies of the crystalline crust have generally been restricted to 2-D surveys, which produce cross-sectional images of the subsurface, the use of industry 3-D seismic reflection data permits the investigation of the deep sill bodies as 3-D features. Following negotiations with BP Canada in 2002, a 3-D data set that overlapped the Winagami sequence was located in the Pine Creek region of northwestern Alberta (Fig. 1). Although the data set was acquired strictly for exploration purposes and so

*Now at: Department of Earth Sciences, Memorial University of Newfoundland St. John's, NL, Canada. E-mail: kwelford@esd.mun.ca

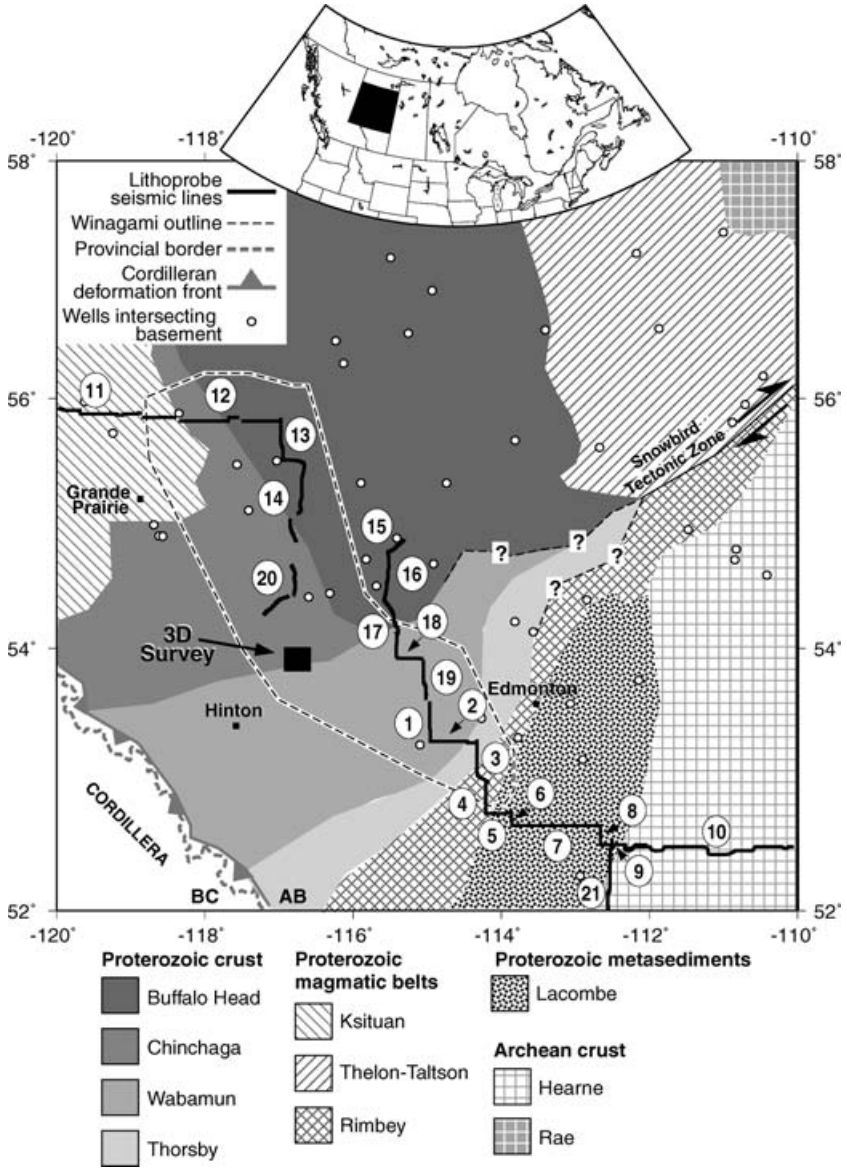

Figure 1. Detailed basement domain map of the region surrounding the Pine Creek 3-D survey area. The locations of the CAT'92 and PRAISE'94 2-D seismic reflection lines collected by Lithoprobe (with line numbers shown in white circles) are also shown. The inferred bifurcation of the Snowbird Tectonic Zone is shown in the eastern part of the map. Basement domains are based on our interpretation of the aeromagnetic data.

was limited to recording times of 5.1 s TWTT (∼15 km depth), the nearby Lithoprobe evidence for the WRS indicated that at least the top of the Winagami complex could be imaged and mapped in 3-D using the Pine Creek data set. This study presents the results of our analyses of this data set. Along with 3-D seismic investigations around the German KTB borehole (Stiller 1991) and studies of the Head-Smashed-In reflector of southern Alberta, Canada (Welford & Clowes 2004), this work represents one of the pioneering efforts to examine upper–middle crustal structure to depths on the order of 15 km using industry-style 3-D seismic reflection data.

2 BACKGROUND INFORMATION

The WRS is observed on four of the ten multichannel Lithoprobe lines from the 1992 Central Alberta Transect (CAT, lines 1–10) experiment and on eight of the ten lines from the 1994 Peace River Arch Industry Seismic Experiment (PRAISE, lines 11–20) (Fig. 1). Confined to the crystalline basement beneath the Western Canada Sedimentary Basin (WCSB), the sill complex extends through several Proterozoic basement domains. Most relevant to the Pine Creek survey are the Wabamun and the Chinchaga domains, ranging in age from 2.0 to 2.4 Ga (Ross 2002). Their boundaries, along with those of most basement domains below the WCSB, have been determined on the basis of aeromagnetic data and K–Ar and U–Pb dating of drill cores that intersect basement (Burwash *et al.* 1962; Ross *et al.* 1991; Villeneuve *et al.* 1993; Pilkington *et al.* 2000). From cross-cutting relationships with dipping crustal fabric and reflection offsets from dated brittle events, the emplacement of the Winagami sill complex is thought to have occurred between 1890 and 1760 Ma (Ross & Eaton 1997). As such, it postdates the assembly of most of the domains in the study region and was perhaps coeval with tectonism associated with the opening and closing of the Thorsby basin/domain to the southeast (Fig. 1). Since the Winagami sills were intruded prior to the deposition of the Western Canada Sedimentary Basin,

their present-day depth distribution between 10 and 20 km does not represent the depth at which they were intruded. Compensating for the thickness of the sedimentary cover and ignoring erosion of the crystalline basement prior to sediment deposition, Ross & Eaton (2002) suggest that sill emplacement occurred between 6.5 and 16.5 km depth, at and above the brittle–ductile transition depending on the geotherm during emplacement.

The emplacement of basaltic rock into the continental upper crust results from the upward transport of magma from the base of the crust or the upper mantle along vertical conduits or dykes. Magma is intruded along a plane perpendicular to the least principal compressive stress (Gretener 1969; Parsons *et al.* 1992) such that extensional environments will favour vertical intrusions while compressional zones will favour horizontal sheet intrusions. According to Zoback *et al.* (1989), most intraplate regions of the world are presently characterized by compressional stress regimes with extension only occurring in thermally uplifted regions. Assuming that such conditions also prevailed during the Proterozoic, occurrences of horizontal sills should be widespread in intraplate regions of Precambrian crust that have experienced magmatism.

The bands of bright reflections making up the WRS are locally horizontal to subhorizontal but together form a large-scale anastomosing fan that converges to the southeast (Ross & Eaton 1997) (Fig. 2). Since tectonic stresses typically are uniform over distances many times the thickness of the elastic part of the lithosphere (down to 10–35 km) (Zoback *et al.* 1989), large-scale intrusional patterns will be dictated by the stress distribution within plate interiors imposed by the regional tectonics. Meanwhile, local stress variations will control the small-scale variations in the intrusional pattern.

Table 1.
Acquisition parameters for the Pine Creek 3-D data set in northwestern Alberta.

Total number of shots	3724
Shot size/source	4 kg dynamite
Shot depth	18 m
Shot interval	140 m
Source line spacing	630 m
Receiver group interval	70 m
Receiver line spacing	560 m
Maximum source–receiver offset	16 190 m
Average source–receiver offset	2904 m
Maximum number of live receiver lines	11
Maximum number of live channels	2410
Geophones per receiver station	6
Geophone spacing	4 m
Sample rate	2 ms
Record length	5.108 s

3 THE PINE CREEK 3-D DATA SET

The Pine Creek 3-D data set was collected by Veritas Energy Services Inc. in 2001 January for BP Canada. The acquisition parameters for this survey are presented in Table 1. The acquisition geometry of the Pine Creek data set is shown in Fig. 3. For this 3-D survey, 3724 shots were recorded by patches of 5–11 receiver lines each consisting of 12–254 receiver groups. Receiver lines were spaced 560 m apart and the receiver groups were connected at a spacing of 70 m. Due to this variable acquisition, each shot was recorded by between 240 and 2410 receiver groups.

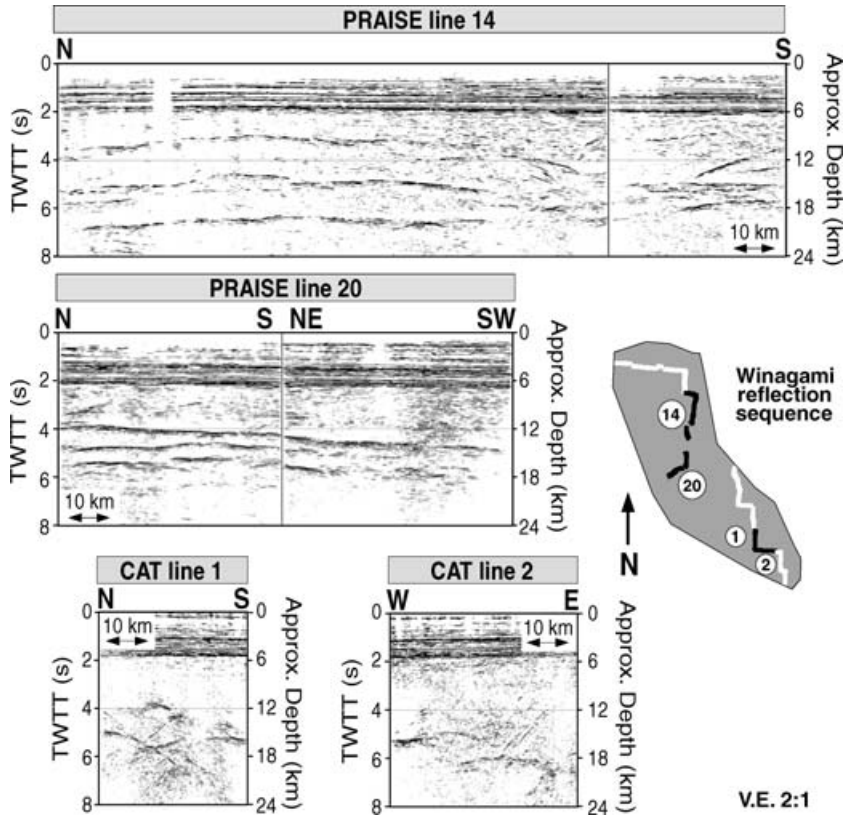

Figure 2. Unmigrated stack of the Winagami reflection sequence on the CAT and PRAISE seismic lines. On all plots, approximate depths are based on an average velocity of 6 km s^{-1}. Since velocities in the sediments are slower, the base of the sediments (which occurs between 1.8 and 2.2 s TWTT on the plots) is not as deep as shown. The seismic lines on which the Winagami is seen are indicated on the location plot. Those displayed are highlighted in black.

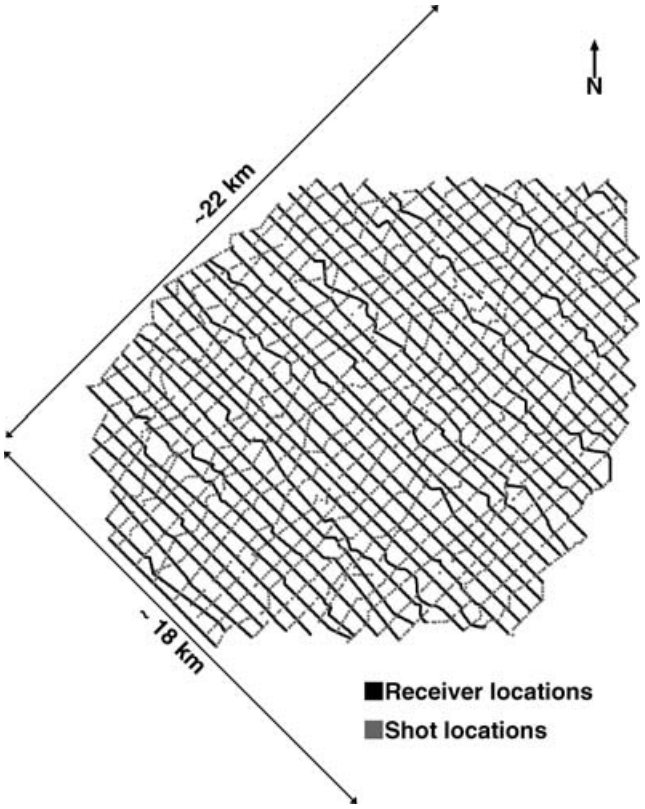

Figure 3. Survey geometry for the Pine Creek 3-D data set.

Data from the Pine Creek survey are of good quality. The processing flow applied to the data set consisted of trace editing, refraction statics, application of a $t^{1.5}$ geometrical spreading correction, spiking deconvolution, NMO correction, residual statics, trace balancing, stack and post-stack 3-D f–k migration (using migration velocity values corresponding to 90 per cent of the average interval velocities computed for the entire data set). To highlight deep reflections in the displayed stacked volume, f–x deconvolution was applied in both the inline and crossline directions.

4 EVIDENCE FOR DEEP REFLECTORS IN THE PINE CREEK REGION

Bright Winagami-like reflections occurring between 4 and 5.1 s TWTT are evident throughout most of the Pine Creek pre-stack data set on both shot and CMP gathers (Fig. 4a). Velocity semblance spectra plots point to high stacking velocities for the deep reflections, which suggest that they originate from within the crystalline basement (Fig. 4b). The deep reflections are unlikely to be originating from scatterers outside the survey area due to their consistent arrival times across the survey and the fact that the apexes of the reflection hyperbolas on both the shot and CMP gathers are generally at or near zero offset.

Throughout the stacked data volume, deep reflections are easily observed between 4 and 5.1 s TWTT on inline (Fig. 5) and crossline (Fig. 6) sections. While the consistency in the arrival times and the relatively high amplitudes of the deep reflections observed on most of the CDP gathers result in brute stacks, which provide an interpretable 3-D image of the deep reflectors, the application of both refraction and residual statics helped improve the reflector's coherency.

Fig. 5 shows six inline sections through the migrated Pine Creek data volume. Progressing from the southwest to the northeast of the data cube (sections a–f), these sections consistently show Winagami-like horizontal to subhorizontal reflections between 4.5 and 5.1 s TWTT. For Sections (a)–(c), the horizontal to subhorizontal reflections are truncated to the southeast. Moving northeast through the volume, Sections (d)–(f) provide a clearer image of a band of

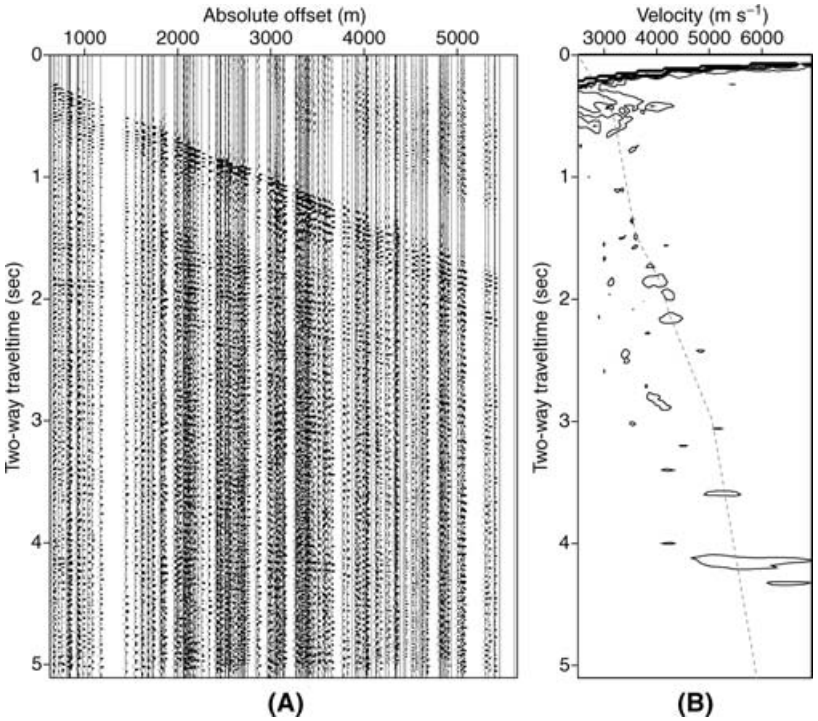

Figure 4. Velocity analysis example for the Pine Creek data set showing (a) a CMP gather, and (b) its semblance velocity spectrum. The picked velocity profile is shown by the dashed light grey line in (b). A 1000-ms AGC gain has been applied to the seismic data plot.

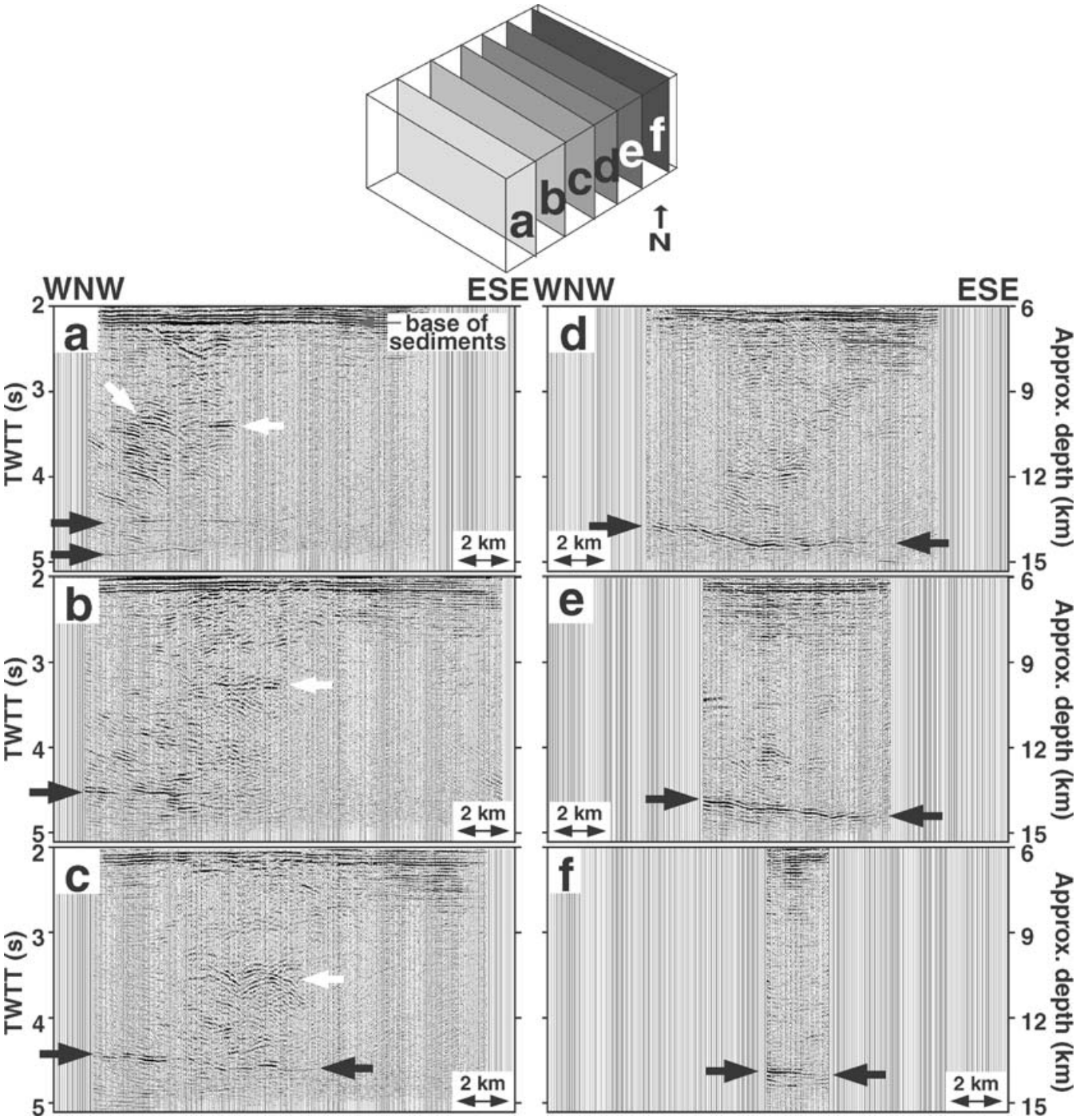

Figure 5. Inline sections through the migrated Pine Creek data volume plotted between 2 and 5.108 s TWTT (approximate depth of 6–15 km). The locations of the sections with respect to the data cube are shown at the top using the lettered labels. The sections have not been horizontally or vertically exaggerated. The locations of the reflections attributed to the Winagami sequence are shown with the black arrows. The smaller white arrows point to shallower instances of basement reflectivity not interpreted to be part of the Winagami sequence. Apart from the geometrical spreading correction, no gain has been applied to the data sections. On all plots, approximate depths are based on an average velocity of 6 km s^{-1}. Since velocities in the sediments are slower, the base of the sediments (which occurs between 2 and 2.5 s TWTT on the plots) is not as deep as shown.

reflectivity dipping to the southeast. On Sections (d) and (e), the reflector appears to have undulating topography. Evidence of a second reflective band is observed at the limits of recorded time on inline Section (a).

The crossline sections shown in Fig. 6 show a coherent reflection at roughly 4.5 s TWTT in the northwesternmost sections (a–c). Moving southeastward (sections d–f), this reflection begins to dip southwestward, eventually disappearing beyond the temporal extent of the recorded traces. Given the southeastward dip of the reflections along the inline sections (Fig. 5), crossline sections further southeast than Section (f) show no Winagami-like reflections. Of note, there is evidence for a second band of reflections at the limits of recorded

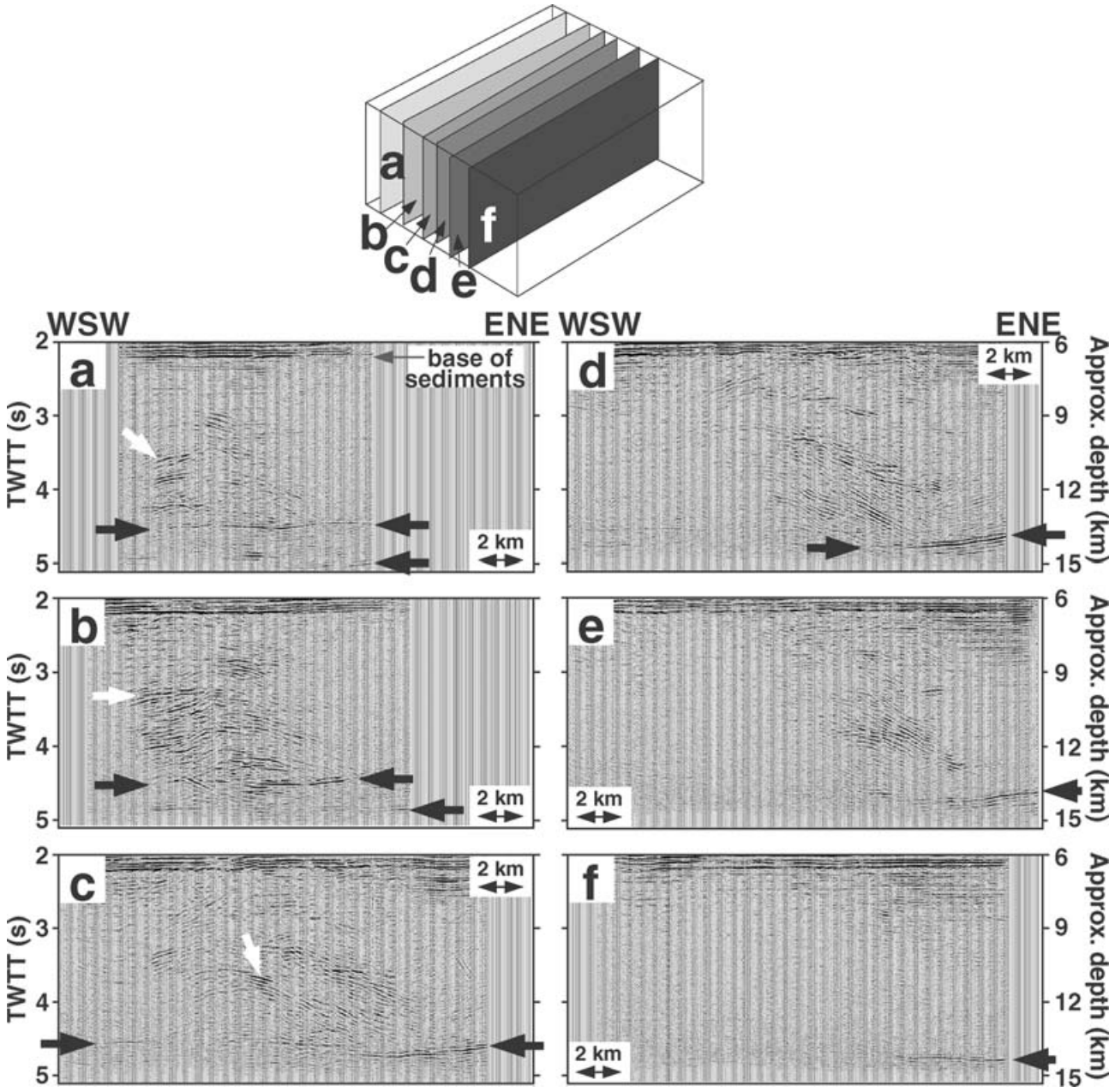

Figure 6. Crossline sections through the migrated Pine Creek data volume plotted between 2 and 5.108 s TWTT (approximate depth of 6–15 km). The locations of the sections with respect to the data cube are shown at the top using the lettered labels. The sections have not been horizontally or vertically exaggerated. The locations of the reflections attributed to the Winagami sequence are shown with the black arrows. The smaller white arrows point to shallower instances of basement reflectivity not interpreted to be part of the Winagami sequence. Apart from the geometrical spreading correction, no gain has been applied to the data sections. On all plots, approximate depths are based on an average velocity of 6 km s^{-1}. Since velocities in the sediments are slower, the base of the sediments (which occurs between 2 and 2.5 s TWTT on the plots) is not as deep as shown.

time on both crossline Sections (a) and (b). If this second band of reflections corresponds to a second sill, the temporal proximity of these reflected arrivals to the overlying ones suggests that the two sill sheets are closer spaced than those imaged to the north by Lithoprobe and that the anastomosing convergence of the sills extends to the base of the 3-D volume.

In Fig. 7, three different chair-cut views through the base of the data volume provide a link between instances of deep reflectivity on the inline, crossline and time sections. In plot a, the crossline section (WSW to ENE) is dominated by a horizontal reflection. The intersection of that reflection with the inline section (WNW to ESE) is suggestive of a sheet dipping to the southeast. Similar patterns are evidenced in plots b and c. In plots b and c, the time slice shows where the sheet cuts through the bottom of the data volume.

The Winagami-like reflections observed throughout the data volume have geometries that greatly differ from the horizontal reflections from the overlying sediments (arriving before 2.5 s TWTT) on all of the vertical data plots. Consequently, the later arrivals are likely not multiples but are reflections that originate from within the crystalline basement. This interpretation is supported by the velocity

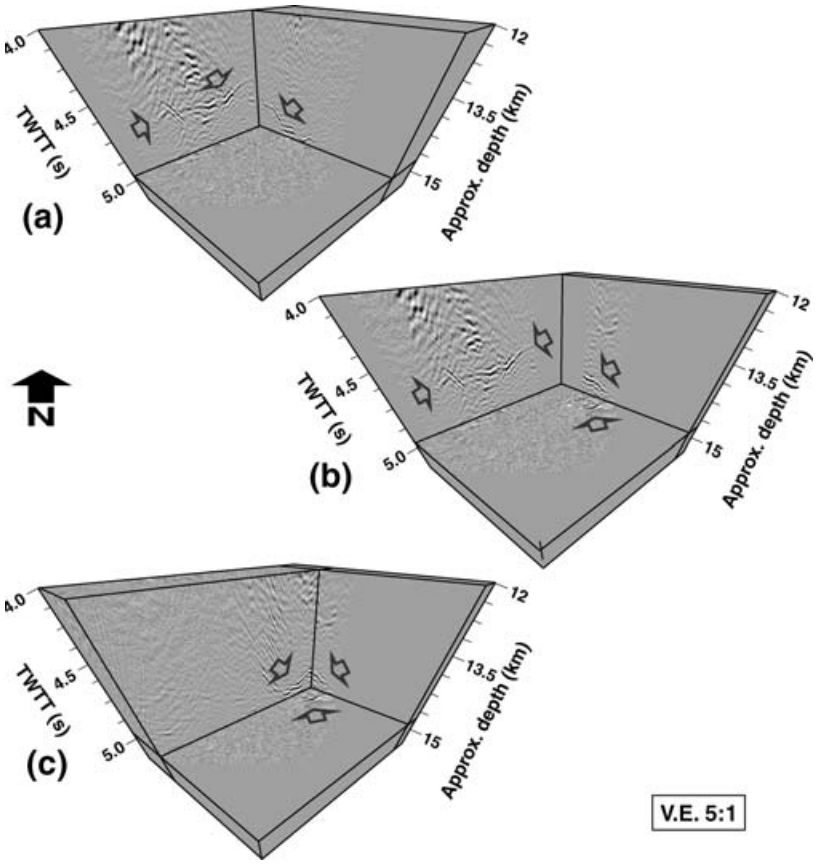

Figure 7. Chair-cut views through the base of the migrated Pine Creek data volume. Arrows indicate regions of coherent reflectivity. Apart from the geometrical spreading correction, no gain has been applied to the data. For all three plots, the portion of the data cube between 4 and 5.1 s TWTT is shown and North points up and into the page. The relative positions of the slices can be deduced by looking at the top of the chair-cut cubes.

analyses that indicated that the deep reflections required higher stacking velocities than the shallower sedimentary arrivals (Fig. 4b).

Reflectivity throughout the data volume is generally quite pronounced although the southeastern portion of the volume is particularly lacking in reflections. Since the amplitudes of the sedimentary arrivals are generally uniform across all the vertical data sections, lateral variations in reflectivity at later times likely represent the true variations in reflectivity.

In all, the Winagami-like reflections in the Pine Creek data volume outline a 3-D reflective surface that is shallowest along the northwest edge of the survey area and dips to the southeast, eventually disappearing beneath the processed data volume. Along the northwestern edge of the data volume, some evidence for a second reflective band is observed although only at the limits of the recorded time.

5 POLARITY CONSTRAINTS

Due to the significant depth at which the WRS resides, no direct physical sampling of the Winagami complex is possible. Nonetheless, further information about the nature of the deep reflectors can be inferred from relationships between the shallow reflections and nearby well logs. Specifically, such comparisons can provide polarity constraints that can help characterize the nature of the impedance contrast from which the reflections have originated.

The Pine Creek survey area has been the focus of oil and gas exploration for over 20 years. Consequently, the area has been densely sampled using well logs. Density and sonic logs for a well at the centre of the survey are shown in Fig. 8(b). The density and sonic logs are multiplied to produce the acoustic impedance log. Furthermore, the density and sonic logs are used to calculate a log of vertical incidence reflection coefficients (*RC*) according to

$$RC = \frac{\rho_2\alpha_2 - \rho_1\alpha_1}{\rho_1\alpha_1 + \rho_2\alpha_2}, \tag{1}$$

where ρ_1, α_1, ρ_2 and α_2 are the density and *P*-wave velocity values above and below the reflective boundary, respectively. Once calculated, the log of reflection coefficients is convolved with a source wavelet to produce a synthetic trace. The source wavelet in Fig. 8(a) was estimated from the amplitude spectrum of the nearest seismic trace to the well location. Only arrivals from the sedimentary sequence corresponding to the sampled depth of the well log were used in the estimation. To determine the appropriate phase for the wavelet, constant phase shifts were applied to the source wavelet until the highest correlation coefficient between the synthetic and recorded trace was obtained. The best match was obtained for a source wavelet with a 154-degree constant phase shift applied, which is why the wavelet is dominated by a negative peak at zero time. With a correlation coefficient of 0.727, both the resulting synthetic trace and the recorded trace correspond well and most reflections can be aligned.

The Nordegg horizon highlighted in Fig. 8(b) marks the transition from overlying low-velocity, low-density shales and sandstones to higher velocity, higher density carbonates, as evidenced by the sharp increases on both the sonic and density logs. These increases result

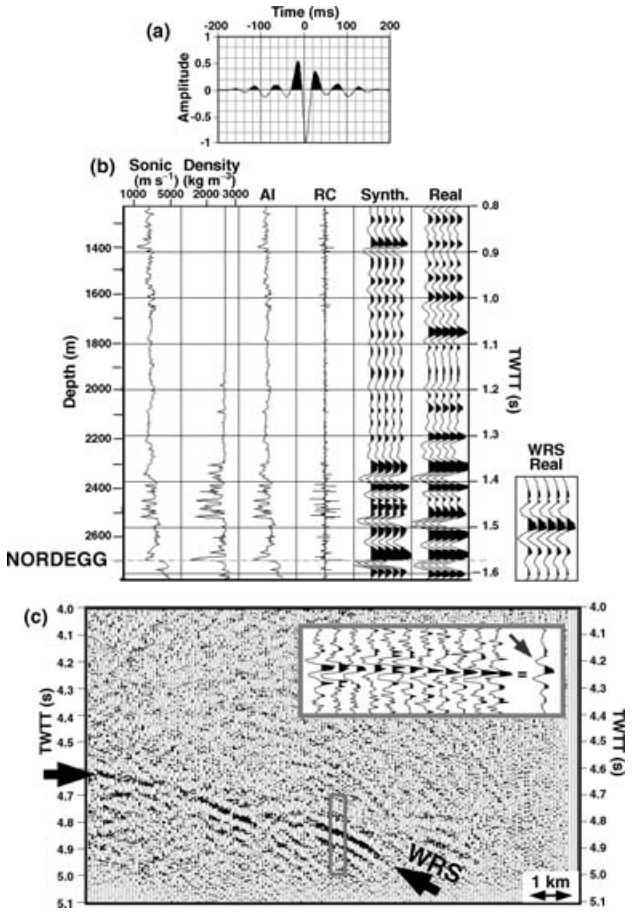

Figure 8. (a) Source wavelet extracted from the stacked trace closest to the well location, (b) well logs from the overlying sedimentary sequence used to obtain polarity constraints for the WRS and (c) an unmigrated inline section through the stacked Pine Creek data volume. In (b), from left to right, the sonic log, bulk density log, a log of acoustic impedance (AI), a log of calculated reflection coefficients (RC), a calculated zero-offset synthetic seismogram (repeated five times for clarity) and the nearest stacked trace to the well location (repeated five times for clarity) for comparison are shown. The highlighted Nordegg horizon, a high velocity/high density contrast with the overlying sediments, is used as the reference horizon and is characterized by a strong negative peak. In (c), a portion of the section outlined by the grey box is enlarged for comparison with the synthetic waveforms in (b). The horizontal stack of these highlighted traces is also plotted for comparison both in the highlighted box and again at the right of (b) (labelled WRS real) where it is repeated five times for clarity and plotted with the same scale as the traces from the sedimentary sequence. The similarity in the reflection character and polarity suggests that the WRS results from a high-velocity/high-density contrast.

in a strong positive reflection coefficient. From the comparison between the synthetic seismogram and the recorded trace, the Nordegg positive reflection coefficient corresponds to a negative peak. This is not surprising given the dominant negative peak at zero time for the source wavelet (Fig. 8a). Assuming that this relationship holds for the entire data volume, positive reflection coefficients should correspond with dominant leading negative peaks throughout the Pine Creek data volume.

The Nordegg horizon and its corresponding logs from Fig. 8(b) are compared against a portion of an unmigrated inline section in Fig. 8(c). An enlarged segment of the stack (outlined in grey) demonstrates that the leading dominant peak for the deep reflection appears negative. This is reinforced by the horizontal sum of the highlighted traces which clearly shows a negative peak as the first dominant arrival (shown by dark grey arrow). If the relationship derived for the Nordegg horizon holds true, the polarity of the deep reflection suggests that it is arising from a positive reflection coefficient. Since doleritic material has both higher velocities and densities than the host granitic gneisses (Juhlin 1990), these results support the interpretation that the reflections are arising from higher density, higher velocity material, possibly doleritic mafic sills. While Henstock & Levander (2000) draw into question the reliability of reflection polarity as an indicator of subsurface contrasts in regions with complex overburden and/or reflective targets, our interpretation of the polarity results is supported by the simple sheet-like geometry of the sill target investigated in this paper and the relatively uniform layering of the overlying sedimentary sequences (Ross & Eaton 2002).

6 1-D WAVEFORM MODELLING

The thickness of the topmost sill body from the WRS was previously estimated at 70 ± 10 m along line 20 of the PRAISE experiment (Ross & Eaton 1997) (Fig. 1). With multiple data sections containing the Winagami-like reflections, the Pine Creek data volume offers an opportunity to examine changes in the reflector's thickness over the span of the survey using 1-D waveform modelling.

Using the wavelet from Fig. 8(a) as the source wavelet, 1-D synthetic seismograms were constructed using a range of different three-layer 1-D models of a sill intruded into a host rock. These synthetic seismograms were then compared with coherent reflections throughout the data volume (Fig. 9). The algorithm for generating the synthetic traces involved computing the reflection coefficients at the appropriate zero-offset traveltimes and convolving them with the source wavelet. Multiples were not included in the generation of the synthetic traces. A similar algorithm was used by Ross & Eaton (1997) to obtain their sill thickness estimate. The host rock and sill material properties were assigned velocity and density values of 6000 m s^{-1} and 2650 kg m^{-3} for the granite, and 6500 m s^{-1} and 3000 kg m^{-3} for the dolerite, respectively (Juhlin 1990). Sill thicknesses ranging from 10 m to 150 m were used to span the range of thicknesses deduced from earlier studies (Ross & Eaton 1997; Mandler & Clowes 1997, 1998).

The horizontal stack of the highlighted traces from the southwestern section (Fig. 9a) reveals a wavelet with two positive peaks flanking a dominant asymmetric negative peak. From comparison with the 1-D modelling results, this wavelet most resembles the results for a sill with a thickness of 110 ± 10 m both in terms of wavelet length and character. For both the middle and northeastern sections, the horizontal stacked traces produce wavelets of similar length and reflective character corresponding to a thickness of 90 ± 10 m. From these combined results, the Winagami sill imaged by the Pine Creek data set is inferred to have a thickness on the order of 100 m throughout the survey area with a slight thickening to the southwest. Since these thickness estimates exceed those obtained to the north by Ross & Eaton (1997), the top sill in the Winagami complex is inferred to thicken towards its southern extent.

7 3-D KIRCHHOFF FORWARD MODELLING

Commercial interpretation software packages for 3-D seismic data volumes are designed to track laterally coherent reflective surfaces within sedimentary sequences for oil and gas exploration. Since

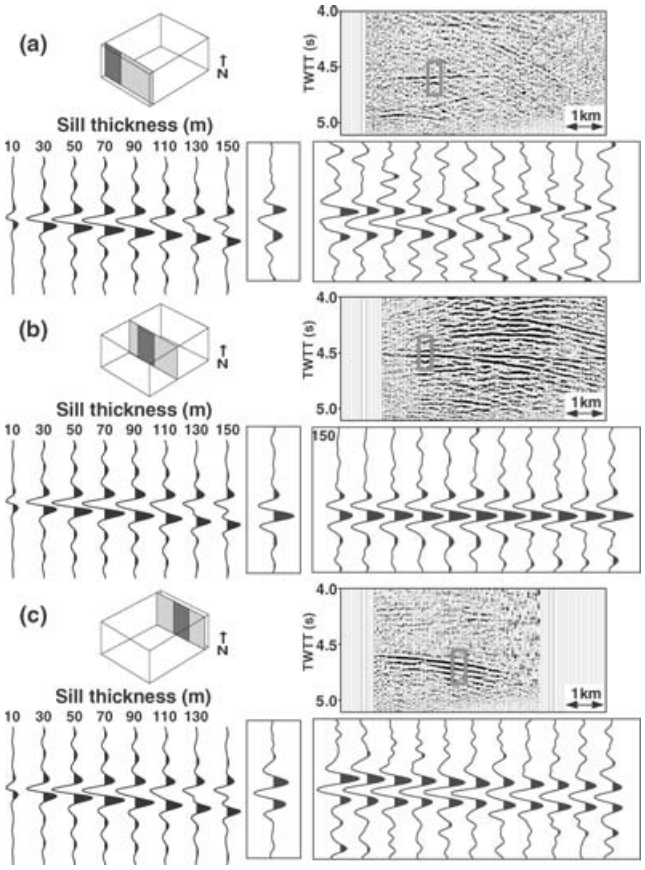

Figure 9. Comparison of 1-D modelling results with coherent reflections from (a) the southwest, (b) the centre and (c) the northeast of the Pine Creek data volume. The 1-D seismograms were computed using the wavelet from Fig. 8(a) and simple three layer models of different thicknesses of dolerite sills emplaced in granite. The models are constructed using velocity and density values of 6000 m s^{-1} and 2650 kg m^{-3} for the granite, and 6500 m s^{-1} and 3000 kg m^{-3} for the dolerite, respectively. For each section, the location of the section (top left with shown data section highlighted in dark grey), the data section (top right), the modelling results (bottom left), the traces highlighted by the grey box in the data section (bottom right), and the horizontal stack of the highlighted traces (bottom centre) are shown. The highlighted traces in the grey boxes were band-pass filtered (5–10–40–50 Hz) to better match the wavelet used to compute the synthetics. The horizontal stacks were computed using the filtered traces. The modelling results and the stacked data are plotted to the same scale.

deep reflections within crystalline basement are generally less coherent, these packages do not provide the proper tools for tracking discontinuous deep reflections in 3-D. Consequently, to validate an interpreted model of the top of the Winagami sill complex based on the migrated results, 3-D forward modelling of the reflector was done using the *kmod3d* code developed by Eaton & Clarke (2000). This efficient program is based on the Kirchhoff integral method and calculates the scattered 3-D wavefield generated by a body of arbitrary shape in a homogeneous elastic medium. The parameters of the wavefield are determined for any point in the medium using the wavefield and its normal derivatives on the closed surface of the scattering body. A number of high frequency assumptions, such as using ray theory in portions of the model where the background medium varies slowly, are made to simplify the solution (Eaton & Clarke 2000).

The parametrization for *kmod3d* involves approximating the surface of the scattering body using plane triangular surface elements (Eaton & Clarke 2000). For each triangle, the wavefield is approximated as a plane wave. The influence of each of the triangle's vertices toward scattering is quantified by a weighting function and the triangle's total contribution is determined by numerical integration.

For modelling the top reflection of the Winagami sequence in the Pine Creek data volume, the scattering surface is simply specified as a layer that extends laterally to the bounds of the model space. While *kmod3d* can handle coarse sampling of the scattering surface on the order of the Fresnel zone radius (approximately 1.5 km for the deep reflections), the model was gridded using a 1 km by 1 km mesh to avoid computational instabilities.

A model with variable sill topography was constructed by picking traveltimes along the top of the reflector sequence for every 20th inline and crossline section through the migrated volume. These picks were then interpolated to produce a 3-D model of the reflector in time. In locations where the deep reflector was not imaged and no pick constraints were available, the traveltimes to the reflector surface were set to greater than 5.1 s TWTT, the temporal extent of the recorded volume. To properly locate the resulting reflections in depth, the velocity of the background medium was set to 5500 m s^{-1}, a depth-weighted average of the interval velocities of the sediments and the basement in the Pine Creek region, these being estimated from the stacking velocities. The contrast in velocities and densities across the scatterer's surface were assigned the same values as were used for the 1-D seismic modelling in the previous section. To reproduce some of the stacked results, coincident source and receiver pairs were located above the sill model at locations corresponding to the CDP bins of the stacked traces to simulate a single channel reflection survey.

The goal of the 3-D modelling of the top of the reflective sheet was to construct a model whose geometry would reproduce the shapes and to some extent the character of selected inline and crossline sections through the stacked volume. By iterative fine adjustments of the geometry of the top of the sill body to improve the arrival times and character of the reflections, a 3-D model of the sill is generated (Fig. 10). Since a data set recorded to 5.1 s TWTT will not contain reflections from reflectors deeper than 16 km, only the portion of the model surface above 16 km depth is shown.

Fig. 11 shows a comparison between inline sections through the stacked Pine Creek data volume and the computed traces for coincident sources and receivers along the same inlines (shown as labelled red lines in Fig. 10). From northeast to southwest (A to D), a good comparison is obtained between the reflection geometries on the stacked and modelled sections. Sections (A) and (B) capture the dip of the reflective sheet while the geometry of the subhorizontal truncated reflections in the southwest (sections C and D) is well reproduced. Small-scale discrepancies between the real and synthetic sections such as missing or fabricated diffractions are directly related to the coarseness of the model parametrization and to the local complexity of the model at the sample points.

Fig. 12 shows the equivalent comparison between crossline sections through the stacked Pine Creek data volume and the computed traces for coincident sources and receivers along the same crosslines (shown as labelled green lines in Fig. 10). Along most of the crosslines, an excellent match is achieved between the modelled and stacked data in terms of both arrival times and the geometry of the reflections. Variations in reflection amplitudes along the profiles result directly from the picked topographical variations along the reflector surface. The lack of recorded coherent reflections along the western end of section (B) may be due to a lack of complexity in the modelled surface at that location. To the southeast, modelled

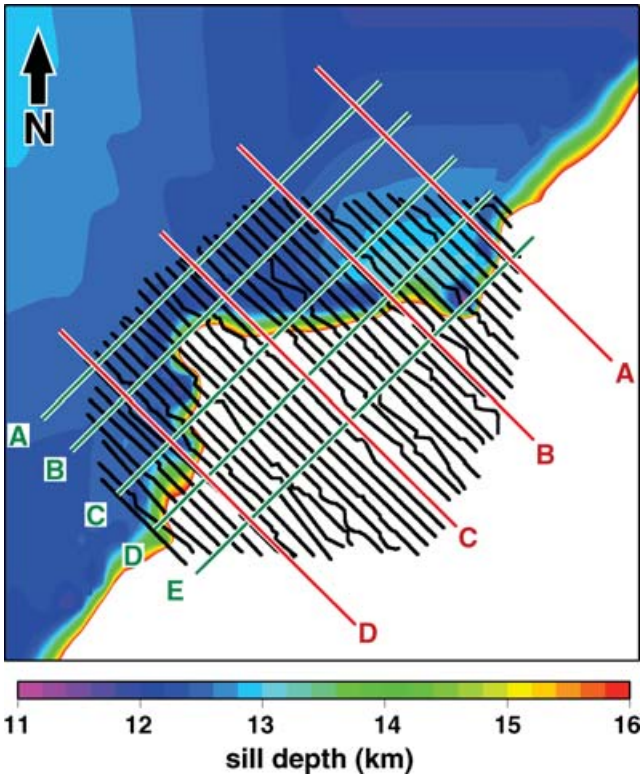

Figure 10. 3-D model of the top of the Winagami sequence from 3-D Kirchhoff forward modelling. Since a data set recorded to 5.1 s TWTT will not contain reflections from reflectors deeper than 16 km, only the portion of the model surface above 16 km depth is shown. For the parametrization, the model surface extended across model space. The locations of the inline model sections from Fig. 11 are shown in red and labelled to correspond with that figure. Similarly, the locations of the crossline model sections from Fig. 12 are shown in green and labelled to correspond with that figure. Receivers lines from the Pine Creek survey are overlain for reference.

crosslines D and E capture the southwestward dip of the reflective surface.

While the interpretation of the *kmod3d* modelling results are non-unique, the final 3-D model does generally reproduce both the geometry and the reflective character of the deep reflections in the stacked volume. Also, the modelling results allow for an estimation of the proper location and geometry of the reflective sheet. They highlight the fortuitous location of the Pine Creek survey for modelling the Winagami sills. Assuming that the reflections continue their southeastward dip as modelled, if the survey were acquired an additional 10 km to the southeast, no evidence for deep Winagami reflections would have been detected.

8 LACK OF REFLECTIVITY IN THE SOUTHEAST

The 3-D forward modelling results reinforce the conclusion that the Pine Creek volume captures reflections from a southeastward dipping reflective sheet, which dips below the limits of recorded time in the southeastern portion of the data volume. In addition to losing the Winagami-like reflections, the southeast portion of the volume beneath the base of the sediments appears devoid of basement reflectivity entirely (Fig. 5).

To quantify this lack of reflectivity and obtain a spatial view of the distribution of reflectivity within the Pine Creek data volume as a whole, a statistical approach to event picking was used (Welford & Clowes 2004). A spatial coherency filter (Kong *et al.* 1985) was applied to data from below the base of the sediments on all the inline and crossline sections in order to automatically extract all linear events that spanned at least 3 km (the approximate Fresnel zone at 4.5 s for a 10 Hz signal in a medium velocity of 5000 m s^{-1}). Once these events were isolated, only linear reflectors from the inlines and crosslines that intersected each other (within $\pm$10 ms) were selected. Common picks that were not bordered by at least one other common pick (within $\pm$20 ms) were subsequently eliminated to impose a minimum areal constraint on the picked common reflectors.

For the Pine Creek migrated data volume between 3.2 and 5.108 s TWTT (below the base of the sediments), a total of 1 600 375 coherent picks were obtained for all the inline sections and 733 906 picks for all the crossline sections. From these, a total of 434 229 common picks were found to intersect within 10 ms of one another. With the added areal constraint of requiring common picks to be bordered by at least one other pick, the number of common picks was reduced to 422 120. The spatial distribution of the number of common picks per stacked trace is shown in Fig. 13(b). The plot clearly reinforces qualitative observations of the seismic plots that the southeast of the survey is devoid of reflections.

Curiously, the aeromagnetic pattern over the survey contains a strong positive anomaly roughly in the location where reflectivity is lost (Fig. 13c). Since the region's distance from the magnetic pole can cause magnetic anomalies to appear shifted laterally or distorted due to phase contributions from the non-vertical dipole (Blakely 1996), the data were reduced to pole using a subroutine provided by Blakely (1996). This transformation readjusts the data to what they would look like if measured at the Earth's pole where the ambient magnetic field is vertical. The ambient magnetic field in the Pine Creek region was taken to have an inclination of 76.5° and a declination of 67.3° (Hope & Eaton 2002). Since the inclination and declination of the remanent magnetic field in the region are unknown, these were assumed to be small and aligned with the ambient field (Pilkington *et al.* 2000). The results of the reduction to pole are shown in Fig. 13(d). From parts B and D from Fig. 13, the lack of reflectivity in the southeast and a corresponding aeromagnetic high appear to somehow be linked. A similar relationship between lack of reflectivity and an aeromagnetic high was observed further north by Ross & Eaton (2002) where the Winagami reflections vanish beneath the aeromagnetically high Kimiwan anomaly, interpreted as basement metasomatism caused by meteoric fluid in an extensional environment (Burwash *et al.* 2000).

From the regional aeromagnetic map (Fig. 13a), the Pine Creek survey appears to be confined within the Wabamun domain (known as the Wabamun High) and does not extend into the aeromagnetically low Chinchaga domain (known as the Chinchaga Low). The Wabamun High is characterized by up to 20 km wide subcircular positive anomalies, which have been interpreted as undeformed magmatic rocks, bordered by narrow lows (Villeneuve *et al.* 1993). Given the abrupt cessation of reflectivity corresponding to the high anomaly in Fig. 13(d), a variety of emplacement scenarios can be envisaged:

(a) the emplacement of the magmatic rocks could have predated the intrusion of the Winagami sills which for some reason were later forced around the magmatic rocks;

(b) the emplacement of the magmatic rocks could have postdated the Winagami sills and so overprinted them or

(c) the emplacement of the sills and the magmatic rocks could have been co-magmatic. While scenarios #2 and #3 are consistent with the abrupt southeastward truncation of Winagami-like

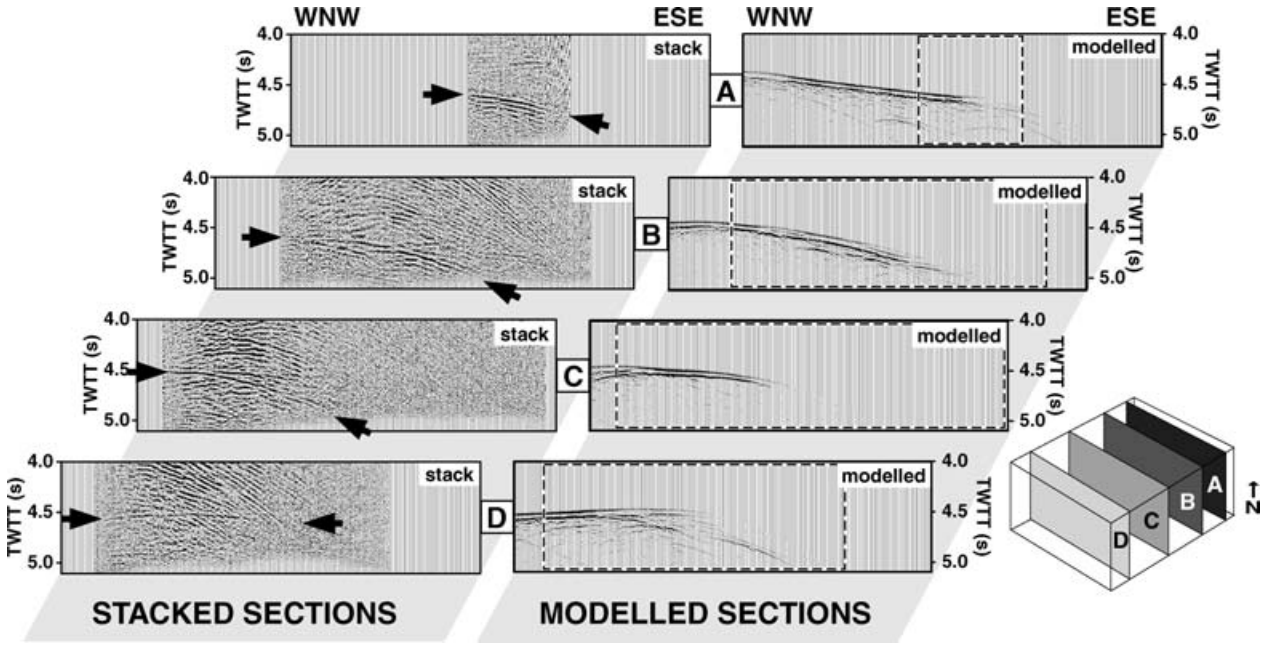

Figure 11. 3-D Kirchhoff forward modelling results for several of the stacked inlines shown in Fig. 5. The locations of the displayed sections with respect to the data cube are shown on the right using the lettered labels. The portions of the modelled sections, which correspond to recorded data coverage are outlined in the dashed boxes.

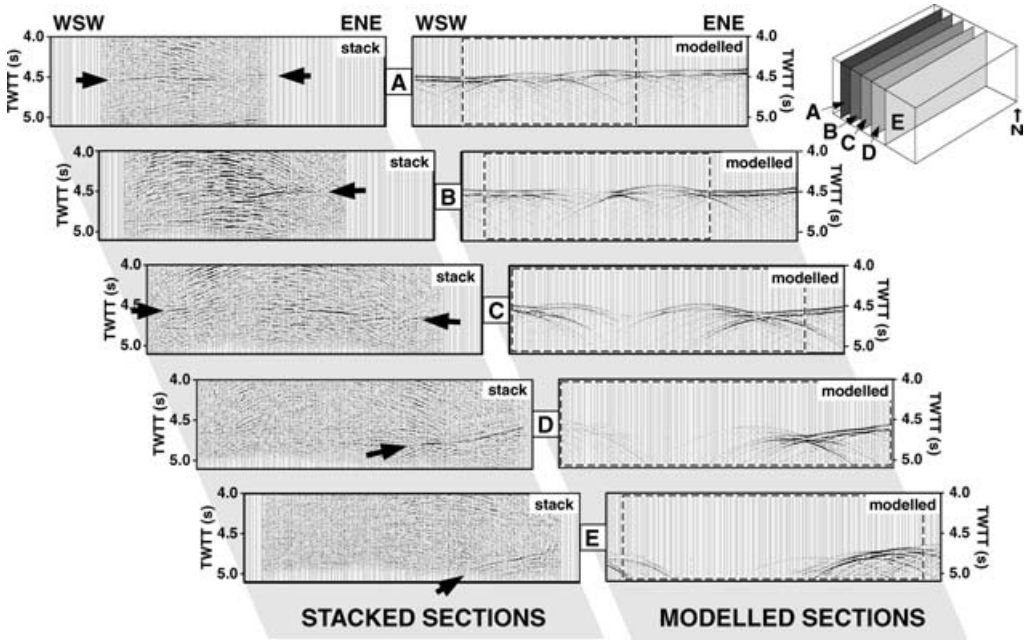

Figure 12. 3-D Kirchhoff forward modelling results for several of the stacked crosslines shown in Fig. 6. The locations of the displayed sections with respect to the data cube are shown on the right using the lettered labels. The portions of the modelled sections, which correspond to recorded data coverage are outlined in the dashed boxes.

reflections in the southwest of the data volume (Fig. 5), the loss of basement reflectivity and the loss of the Winagami reflections may in fact be due to some kind of preferential attenuation of the reflected energy at some shallower depth.

Unfortunately, there is no conclusive way to determine why the southeast of the Pine Creek data volume is lacking in reflectivity. While the zone without reflectivity corresponds presently with an aeromagnetic high, with only one basement drill core dated at 2.3 Ga from the southeastern portion of the Wabamun domain (Villeneuve *et al.* 1993), inferences made about the composition and age of the aeromagnetic highs in the region are purely speculative.

9 DISCUSSION

Following from the previous interpretation for the WRS (Ross & Eaton 1997) and based on the results presented in this paper, the

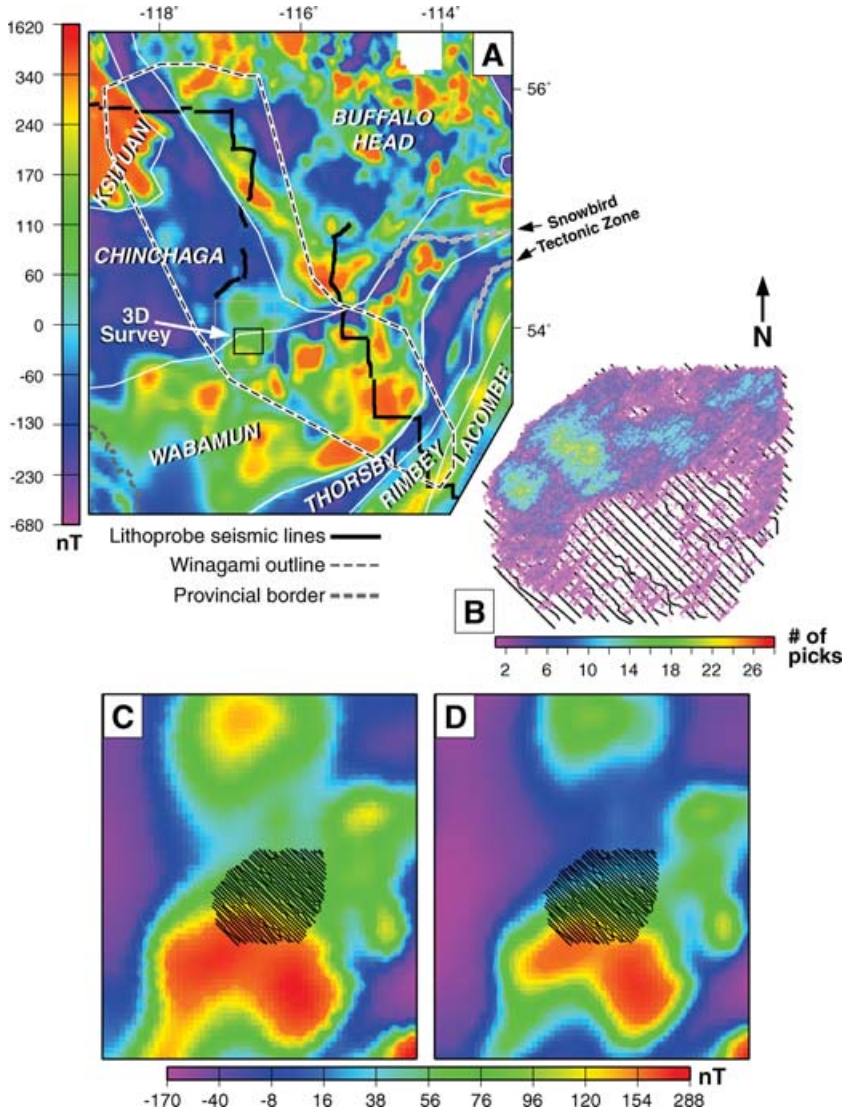

Figure 13. (a) Interpreted aeromagnetic map over the WRS of northwestern Alberta; (b) spatial distribution of the number of reflector picks common to both inline and crossline sections per stacked trace (see text for details); (c) aeromagnetic signal over the Pine Creek survey area and (d) reduced to pole aeromagnetic signal over the Pine Creek survey area. The Pine Creek acquisition geometry is shown on all plots for reference. In (a), a gap in data coverage in the north is left blank. White lines show basement domain boundaries inferred from the aeromagnetic signatures. For reference, the Lithoprobe seismic reflection lines are also shown. The black box outlines the Pine Creek survey area. The thin grey box outlines area of map shown in (c) and (d). The inferred bifurcation of the Snowbird Tectonic Zone is plotted as the thick dashed grey lines in the eastern part of the map.

mafic sill interpretation for the Winagami reflections is supported. While polarity constraints would also be consistent with a mylonitic shear zone as the source of the reflections, the sill interpretation is preferred based on the sharpness of the reflections, the consistency of the waveform throughout the data volume and the locally variable geometry of the reflections.

The Winagami sill complex is inferred to have been emplaced into a rheologically layered upper–middle crust under horizontal compression (Ross & Eaton 1997). From timing constraints and from high upper crustal RMS velocities obtained to the northeast of the Winagami sequence from the refraction/wide-angle reflection Peace River Arch Seismic Experiment, PRASE (Zelt & Ellis 1989), Ross & Eaton (2002) proposed that this compression resulted from the brittle indentation of the Slave province into the Rae province to the northeast. This collision was accompanied by temporally sporadic but regionally extensive magmatism mostly evidenced as vertical dyke intrusions (Ross & Eaton 1997). While plausible, this inferred emplacement scenario does not easily explain the unusual southeastward-converging anastomosing shape of the WRS evidenced by both the Lithoprobe results (Fig. 2) and those presented in this paper (Fig. 5).

As outlined in the background information, magma will intrude along a plane perpendicular to the least principal compressive stress (Gretener 1969; Parsons *et al.* 1992). Consequently, compressional zones will favour horizontal sheet intrusions. However, in addition to the regional stresses, the emplacement of a sill will alter the stress field locally such that the stresses perpendicular to the sill propagation direction will increase. Thus, nearby sills propagating parallel will be deflected away from each other as they each seek out an orientation that better favours the opening of cracks (Pollard 1973). Based on this scenario, the magmatic source for the Winagami sills must be located in the southeast and the sills must

have diverged as they propagated to the northwest. Such a propagation direction contradicts the interpretation by Ross & Eaton (1997) that the indentation of the Slave province into the Rae province was the source of the magmatism. In order to reconcile a source of magmatism in the northeast and the anastomosing shape of the Winagami reflectors, the sills must converge as they propagate southeastward.

From mechanical modelling results, Pollard (1973) outlined three conditions under which sills could converge:

(1) if the host rocks are strongly anisotropic and thus control the path of intrusion
(2) if there is a time gap between the intrusion of individual sills such that the applied stress can relax between intrusions
(3) if the sills encounter regional extension normal to the propagation direction, which favours the opening of cracks.

Based on numerical simulations of vertical fluid-filled dykes propagating and converging towards the topographic load of a volcano (Dahm 2000), a fourth condition for convergence can be envisaged. In this scenario, horizontal sills propagate towards an increased and localized maximum compressive stress such that the stresses that neighbouring sills impose on each other are negligible in comparison. This compressive stress would have to be concentrated in the mid-crust.

In order for the southward propagation of the Winagami sills to be plausible, at least one of the four proposed conditions for convergence must be satisfied. Since the basement rocks into which the WRS was intruded are generally gneissic, metamorphic segregation and banding of minerals may have imparted an anisotropy into the upper crust, which controlled the direction of emplacement. From drillcore evidence from several of the basement domains, both weak and strong foliations are observed which could support this scenario (Villeneuve *et al.* 1993). Thus, condition #1 is plausible. Since the only way to discount condition #2 involves drilling to the sills and dating them, in the absence of contradictory evidence, it remains a viable contender to support a southward propagation of the sills. Meanwhile, tectonic candidates for satisfying conditions #3 and/or #4 can be investigated by examining the regional tectonic activity during emplacement.

9.1 Regional tectonic activity during emplacement

The tectonic assembly of northwestern Alberta took place during the Paleoproterozoic in three general regions separated by the Great Slave Lake shear zone in the north and the enigmatic Snowbird Tectonic Zone in the south (Ross 2002) (Fig. 14). In the central block, by 1980 Ma, the Buffalo Head and Chinchaga domains acted as one unit flanked to the east and west by outward dipping subduction zones (Ross 2002; Ross & Eaton 2002). By 1940 Ma, the Buffalo Head–Chinchaga domain was sutured to the Thelon–Taltson belt (Ta, T) in the east while subduction continued in the west. By 1900 Ma, the Buffalo Head–Chinchaga domain had been sutured to the continent, while to the south, extension was initiated as a result of the counter-clockwise rotation of the Hearne province in response to plate consumption in the southeast as part of the Trans-Hudson Orogen (Ross *et al.* 2000; Ross & Eaton 2002). At 1850 Ma, a possible emplacement time for the Winagami sequence, the greatest amount of tectonic activity in the region was occurring south of the Snowbird Tectonic Zone. As the plate consumption in the Trans-Hudson Orogen continued, the Thorsby ocean basin was rifted open between the Wabamun domain and the Hearne province. By 1800 Ma, the cessation of Trans-Hudson plate consumption resulted in the Hearne province moving northwestward again and consequently the Thorsby basin/domain was partially subducted under the Hearne forming the Rimbey granites. This tectonic framework does not provide an obvious candidate to satisfy condition #3 since the opening of the Thorsby basin would have favoured the intrusion of vertical dykes. However, the corresponding northwestward ridge push from the cooling and gravitational collapse of the rocks of the new oceanic crust could have satisfied condition #4 by providing a localized and increased compressive stress towards which the sills could have propagated. If correct, this scenario could further constrain the timing of emplacement of the Winagami sequence to between 1890 and 1850 Ma, synchronous with the opening of the rift basin.

The temporal overlap between the opening of the Thorsby basin and the emplacement of the Winagami sill complex may however point to the rifting itself as the source of the magmatism. Such a scenario would more easily explain the anastomosing shape of the sills as they diverged northwestward during emplacement and would also explain the apparent thickening of the sills in the southeast. However, since no direct methods are available to confirm that the conditions necessary for sill convergence were not satisfied for the emplacement of the Winagami sequence, southeastward sill convergence cannot be ruled out. This possibility coupled with the higher upper crustal velocities to the north and the coeval magmatism associated with the indentation of the Slave province into the Rae province are suggestive of a source of magmatism to the northeast of the imaged extent of the intrusions. If so, the sill thickness increase in the 3-D volume relative to the Lithoprobe results to the north may simply reflect variations in the compressibility and density of the Chinchaga and Wabamun domain basement rocks that directly influenced the nature of the sill emplacement.

While the emplacement of sills is often argued to correspond with the existence of a mafic underplate at the base of the crust (Nelson 1991), no underplate has been recognized in the Winagami region and its magmatic influence appears limited to the upper crust (Ross 2002). As argued by Ross & Eaton (2002) on the basis of results from Ernst & Buchan (2001), the lack of an associated underplate does not preclude its existence but may indicate that the magmas travelled a great distance from their source. Alternatively, the feeder system for the Winagami sill complex may have involved a larger number of narrow vertical dykes that efficiently distributed the magma through the crust without the ponding at the base of the crust associated with underplate formation. While such vertical features would not be detectable on near-vertical seismic reflection data, the tops of these dykes could be responsible for instances of localized, discontinuous reflectivity within the crystalline crust (indicated by white arrows in Figs 5 and 6 and also evidenced by the pockets of multiple common reflector picks in Fig. 13b).

10 CONCLUSIONS

Using a data set collected by the Canadian petroleum industry in northwestern Alberta, a Precambrian sill complex within the crystalline upper crust, first identified along Lithoprobe 2-D multichannel seismic reflection profiles, is investigated in 3-D. Clear evidence of the WRS (Ross & Eaton 1997) emerges from the data set acquired to 5.1 s TWTT (∼15 km depth). Deep reflections recorded along inline, crossline and time sections of the data reveal a 3-D reflective sheet dipping to the southeast. Polarity comparisons of known reflections from within the sedimentary sequence indicate that a reflective body of higher density and higher velocity than

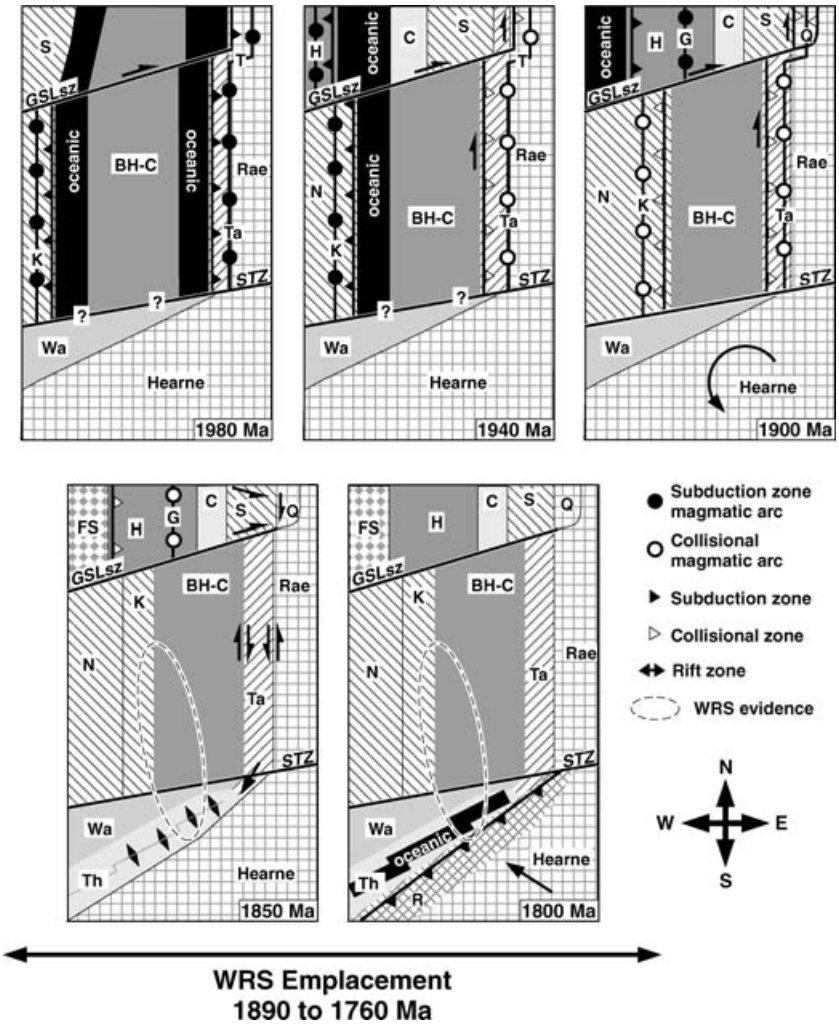

Figure 14. Tectonic evolution of northwestern Laurentia from 1980 to 1800 Ma. The figure was inspired and adapted from Ross (2002). Further description of the figure is provided in the text. Tectonic domains and features: BH-C, Buffalo Head–Chinchaga domain; C, Coronation supergroup; FS, Fort Simpson terrane; G, Great Bear magmatic arc; GSLsz, Great Slave Lake shear zone; H, Hottah magmatic arc; K, Ksituan magmatic arc; N, Nova domain; Q, Queen Maud uplift; R, Rimbey granites; S, Slave province; STZ, Snowbird Tectonic Zone; T, Thelon magmatic arc; Ta, Taltson magmatic arc; Th, Thorsby domain; Wa, Wabamun domain.

the surrounding gneissic basement is responsible for the deep reflections. Such a finding is consistent with the earlier interpretation that the WRS represents doleritic sills (Ross & Eaton 1997). Simple 1-D forward modelling results reveal that the thickness of the sheet is on the order of 100 m throughout the survey region. From 3-D Kirchhoff forward modelling, the geometry of the reflective sheet is constrained and found to exist between approximately 11 and 16 km depth beneath the survey area. Deeper evidence of the reflective sheet is unavailable due to the limited recording time. Comparison of the distribution of reflectivity within the data volume and the regional aeromagnetic pattern reveal that the absence of Winagami reflections, and basement reflectivity in general, coincides with a positive aeromagnetic anomaly, previously interpreted as corresponding to magmatic rocks. The emplacement of the magmatic rocks could have preceded, postdated or been co-magmatic with the emplacement of the Winagami sills. Alternatively, the loss of reflectivity for both may be due to preferential attenuation of the reflected energy at some shallower depth. The anastomosing shape of the Winagami reflections is used to argue the case for two possible directions of emplacement. Since neither direction can be refuted based on available evidence, the magmatism source in the northeast and the southward propagation direction suggested by Ross & Eaton (2002) is preferred. It is also possible that the Winagami sequence was emplaced locally by numerous vertical feeder dykes distributed throughout the crust.

This paper demonstrates that 3-D seismic reflection data sets collected by the petroleum industry can contain meaningful information for tectonic investigations of the upper crystalline crust if they are recorded to adequate times. Communication between industry and academia is essential to isolating future deep targets of interest and to ensuring that data are acquired to sufficiently long listening times so as to allow academic studies of the crust below the sedimentary section.

ACKNOWLEDGMENTS

We thank BP Canada for donating data from the Pine Creek 3-D survey and for permission to publish the results, Kelman Archives for providing the data to UBC and LogTech Canada Limited for donating the well logs. We are also thankful to Prof David W. Eaton for providing the 3-D modelling code and to Prof Don Lawton for

allowing us to perform the 3-D migration of the data at the University of Calgary. Constructive comments provided by two anonymous reviewers were much appreciated. Research support for this project derived from a Science and Engineering Research Canada (NSERC) Discovery Grant to RMC.

REFERENCES

Blakely, R.J., 1996. *Potential Theory in Gravity and Magnetic Applications*, Cambridge University Press, Cambridge, 461 pp.

Burwash, R.A., Baadsgaard, H. & Peterman, Z.E., 1962. Precambrian K-Ar dates from the Western Canada Sedimentary Basin, *J. geophys. Res.,* **67,** 1617–1625.

Burwash, R.A., Chacko, T., Muehlenbachs, K. & Bouzidi, Y., 2000. Oxygen isotope systematics of the Precambrian basement of Alberta: implications for Paleoproterozoic and Phanerozoic tectonics in northwestern Alberta, *Can. J. Earth. Sci.,* **37,** 1611–1628.

Coffin, M.F. & Eldholm, O., 1994. Large igneous provinces: crustal structure, dimensions, and external consequences, *Rev. Geophys.,* **32,** 1–36.

Dahm, T., 2000. Numerical simulations of the propagation path and the arrest of fluid-filled fractures in the Earth, *Geophys. J. Int.,* **141,** 623–638.

Eaton, D.W. & Clarke, G., 2000. *A Kirchhoff integral method to model 3-D elastic-wave scattering*, 70th Ann. Int. Meeting of the Soc. Expl. Geophys. Expanded Abstracts.

Ernst, R.E. & Buchan, K.L., 2001. The use of mafic dyke swarms in identifying and locating mantle plumes, in *Mantle Plumes: Their Identification Through Time*, eds Ernst, R.E. & Buchan, K.L., pp. 247–265, *Geol. Soc. Am.,* Special Paper 352.

Gretener, P.E., 1969, On the mechanics of the intrusion of sills, *Can. J. Earth. Sci.,* **6,** 1415–1419.

Henstock, T.J. & Levander, A., 2000. Impact of a complex overburden on analysis of bright reflections: a case study from the Mendocino Triple Junction, *J. geophys. Res.,* **105,** 21 711–21 726.

Hope, J. & Eaton, D.W., 2002. Crustal structure beneath the Western Canada Sedimentary Basin: constraints from gravity and magnetic modelling, *Can. J. Earth. Sci.,* **39,** 291–312.

Juhlin, C., 1990. Interpretation of the reflections in the Siljan Ring area based on results from the Gravberg-1 borehole, *Technophysics,* **173,** 345–360.

Kong, S.M., Phinney, R.A. & Roy-Chowdhury, K., 1985. A nonlinear signal detector for enhancement of noisy seismic record sections, *Geophysics,* **50,** 539–550.

Mandler, H.A.F. & Clowes, R.M., 1997. Evidence for extensive tabular intrusions in the Precambrian shield of western Canada: a 160-km-long sequence of bright reflections, *Geology,* **25,** 271–274.

Mandler, H.A.F. & Clowes, R.M., 1998. The HSI bright reflector: further evidence for extensive magmatism in the Precambrian of western Canada, *Tectonophysics,* **288,** 71–81.

Nelson, K.D., 1991. A unified view of craton evolution motivated by recent deep seismic reflection and refraction results, *Geophys. J. Int.,* **105,** 25–35.

Parsons, T., Sleep, N.H. & Thompson, G.A., 1992. Host rock rheology controls on the emplacement of tabular intrusions: implications for underplating of extended crust, *Tectonics,* **11,** 1348–1356.

Pilkington, M., Miles, W.F., Ross, G.M. & Roest, W.R., 2000. Potential-field signatures of buried Precambrian basement in the Western Canada Sedimentary Basin, *Can. J. Earth. Sci.,* **37,** 1453–1471.

Pollard, D.D., 1973. Derivation and evaluation of a mechanical model for sheet intrusions, *Tectonophysics,* **19,** 233–269.

Ross, G.M., 2002. Evolution of Precambrian continental lithosphere in western Canada: results from Lithoprobe studies in Alberta and beyond, *Can. J. Earth. Sci.,* **39,** 413–437.

Ross, G.M. & Eaton, D.W., 1997. Winagami reflection sequence: Seismic evidence for postcollisional magmatism in the Proterozoic of western Canada, *Geology,* **25,** 199–202.

Ross, G.M. & Eaton, D.W., 2002. Proterozoic tectonic accretion and growth of western Laurentia: results from Lithoprobe studies in northern Alberta, *Can. J. Earth. Sci.,* **39,** 313–329.

Ross, G.M., Parrish, R., Villeneuve, M. & Bowring, S., 1991. Geophysics and geochronology of the crystalline basement of the Alberta Basin, western Canada, *Can. J. Earth. Sci.,* **28,** 512–522.

Ross, G.M., Eaton, D.W., Boerner, D.E. & Miles, W., 2000. Tectonic entrapment and its role in the evolution of the continental lithosphere: an example from the Precambrian of western Canada, *Tectonics,* **19,** 116–134.

Stiller, M., 1991. 3-D vertical incidence seismic reflection survey at the KTB location, Oberpfalz, in *Continental lithosphere: deep seismic reflections*, eds Meissner, R., Brown, L., Durbaum, H.-J., Franke, W., Fuchs, K. & Seifert, F., *Geodyn. Ser. 22*, pp. 101–114, AGU, Washington, DC.

Theriault, R.J. & Ross, G.M., 1991. Nd isotope evidence for crustal recycling in the ca. 2.0 Ga subsurface of western Canada, *Can. J. Earth. Sci.,* **28,** 1140–1147.

Villeneuve, M.E., Ross, G.M., Theriault, R.J., Miles, W., Parrish, R.R. & Broome, J., 1993. Tectonic subdivision and U-Pb geochronology of the crystalline basement of the Alberta Basin, western Canada, *Geol. Surv. Can. Bull.,* **447,** 86 pp.

Welford, J.K. & Clowes, R.M., 2004. Deep 3-D seismic reflection imaging of Precambrian sills in southwestern Alberta, Canada, *Tectonophysics,* **388,** 161–172.

Zelt, C.A. & Ellis, R.M., 1989. Seismic structure of the crust and upper mantle in the Peace River Arch region, Canada, *J. geophys. Res.,* **94,** 5729–5744.

Zoback, M.L. *et al*., 1989. Global patterns of tectonic stress, *Nature,* **341,** 291–298.